Abstract

In recent decades, the central North Sea has been experiencing a general trend of decreasing dissolved oxygen (O_2) levels during summer. To understand the potential causes driving lower O_2, we investigated a three-day period of summertime turbulence and O_2 dynamics in the thermocline and bottom boundary layer (BBL). The study focuses on coupling biogeochemical processes with physical transport processes to identify key drivers of the O_2 and organic carbon turnover within the BBL. Combining our flux observations with an analytical process-oriented approach, we resolve the key drivers that ultimately determine the BBL O_2 levels. We report substantial turbulent O_2 fluxes from the thermocline into the otherwise isolated bottom water which is attributed to the presence of a baroclinic near-inertial wave. This ephemeral contribution to the local bottom water O_2 and carbon budgets has been largely overlooked and is shown to play a role in promoting high carbon turnover in the bottom water throughout the stratification period while simultaneously maintaining high O_2 concentrations. However, this process could become suppressed with warming climate. We propose migrating algal species, favoured by higher water temperature and suppressed turbulence, could out-compete other species for light and nutrients, and shift the oxygen production zone higher up within the thermocline while maintaining similar organic carbon export to the bottom water. Therefore an upward shift in the production layer could lead to further isolation of the bottom water and thus further promote the seasonal occurrence of lower O_2 concentrations.

1 Introduction

1.1 Hypoxia in shelf seas and coastal regions

The distribution of dissolved oxygen (O_2) in marine systems results from the complex interaction between biological processes (photosynthesis and respiration) and physical processes (O_2 flux pathways) occurring within the water column and at the seafloor. O_2 is therefore regarded as an important indicator of ecosystem functioning for aquatic organisms (Best et al., 2007) as well as for benthic activity (e.g., Glud, 2008). Changes in the O_2 distribution, concentrations and supply can therefore have severe impacts on the shelf ecosystems. O_2 concentration below 62.5 μmol L^{-1}, which is generally regarded as the threshold of hypoxia (Vaquer-Sunyer and Duarte, 2008), is shown to impose significant stress on aquatic communities leading

to increased mortality among fish communities (Diaz, 2001). This also highlighted not only the ecological but also the economic impacts of O_2 depletion, leading to increasing concern regarding the occurrence of hypoxia and hypoxic events. In fact, as reviewed by Diaz and Rosenberg (2008), hypoxia in coastal environments is spreading and so are the reports of unprecedented occurrence of hypoxia in several shelf seas and coastal regions (Grantham et al., 2004; Chan et al., 2008; Crawford and Pena, 2013).

1.2 Hydrodynamics and oxygen depletion in the North Sea

The North Sea is situated in the North–West European continental shelf, between the British Islands and continental Europe. Its semi-enclosed basin covers an area of 575'300 km^2, which has an average depth of 74 m and a general decrease in depth from North to South (Otto et al., 1990). The center region is characterized by the presence of the Dogger Bank, a shallow sandbank that also acts as a hydrological divide. The northern and central North Sea hydrology is mainly dominated by inflow from the North Atlantic Ocean at the northern open boundary, while the southern part relies on inflow from the English Channel (Thomas et al., 2005). The Northern and central North Sea areas are also characterized by the occurrence of seasonal water column stratification. Taken together with weak wind-driven residual currents (Otto et al., 1990), this can lead to isolation of central North Sea bottom water that promotes O_2 depletion.

Indeed, in the central North Sea the occurrence of low O_2 levels in bottom waters has already been reported in the past (e.g., North Sea Task Force, 1993; Greenwood et al., 2010). More recently, monitoring studies in the central North Sea for the 2007 – 2008 period have shown that O_2 concentration in the bottom waters at the Oyster Grounds and North Dogger can drop as low as 163 – 169 μmol L^{-1} (60 – 63% saturation) and ~200 μmol L^{-1} (71% saturation), respectively (Fig. 1; Greenwood et al., 2010). Comparable field observations were also reported in the summer of 2010 (Queste et al., 2013). The authors also reviewed the available historical O_2 data in the North Sea (1900 – 2010), revealing a clear increase in O_2 depletion after 1990.

While the reported O_2 levels were still above the hypoxic threshold, growing concerns of hypoxia developing in the North Sea have highlighted the need for more detailed studies on the O_2 dynamics and driving forces (Kemp et al., 2009). In fact, since 1984, surface water temperatures in the North Sea have increased by 1 – 2°C,

68 greater than the global mean (OSPAR, 2009, 2010; Meyer et al., 2011). On seasonal
69 time scales, climate projections indicate longer durations of the stratification period
70 and stronger thermocline stability (Lowe et al., 2009; Meire et al., 2013), with some
71 projection also suggesting earlier onset of stratification (e.g., Lowe et al., 2009). Due
72 to the semi-enclosed nature of the North Sea, earlier onset and longer stratification
73 increases the length of time that the deep water is isolated, potentially allowing lower
74 O_2 concentrations to develop (Greenwood et al., 2010).
75
76 **1.3. Physical controls on oxygen dynamics**

77 The distribution of O_2 and the other dissolved constituents within aquatic
78 systems are largely dictated by physical transport processes. These include the wind
79 driven air – water gas exchange (Wanninkhof, 1992) at the sea surface, molecular
80 diffusion at the sediment – water interface (Jørgensen and Revsbech, 1985),
81 horizontal advection (e.g., Radach and Lenhart, 1995) and turbulent transport in the
82 water column, where the latter transport was reported to significantly contribute to
83 constituent balances (see Rippeth, 2005; Fischer et al., 2013; Kreling et al., 2014;
84 Brandt et al., 2015). In shelf seas, the seasonal occurrence of steep thermoclines acts
85 as an important physical barrier separating the surface layer from nutrient-rich deeper
86 waters (Sharples et al., 2001). As measurements of shear and stratification have
87 shown that the central North Sea thermocline is in a state of marginal stability (van
88 Haren et al., 1999), additional sources of shear could trigger shear instability leading
89 to local production of turbulence within the thermocline. This enhanced local
90 turbulence would subsequently enhance the vertical exchange of constituents such as
91 O_2, organic carbon and nutrients. Therefore, resolving the processes that drive
92 diapycnal (i.e., vertical) fluxes across the thermocline throughout the stratification
93 period is key to understanding the biogeochemical functioning of shelf seas (e.g.,
94 Sharples et al., 2001).
95
96 **1.4 Present study**

97 The goal of this study is therefore to obtain a snap-shot of key turbulent
98 processes driving the O_2 fluxes across the thermocline. We investigate and describe
99 key processes driving the O_2 flux to the bottom waters during the period of our
100 investigation, and how this could potentially influence the seasonal O_2 balance. Using

101 the resolved O_2 flux, we perform a simple 1-D mass balance model to quantify the O_2
102 sources and sinks, and loss in the water column. Finally, we propose processes that
103 could promote hypoxia development in the central North Sea in a warming climate.
104
105 ## 2 Methods
106 ### 2.1 Study site
107 We performed our O_2 and turbulence measurements campaign in the
108 Norwegian sector of the central North Sea, N. 1/9, at the Tommeliten site (56°29'30"
109 N, 2°59'00" E; Fig. 1) over a time period of three days during the stratification period
110 (8 – 11 August 2009) aboard the R/V *Celtic Explorer* (cruise CE0913). The site,
111 located ~100 km northeast from the northern Dogger Bank, and its surroundings are
112 characterized by shallow waters (~70 m) at a relatively long distance from coastal
113 areas (on average ~300 km). The site is known for the presence of buried salt diapirs,
114 methane (CH_4) seeps and bacterial mats (Hovland and Judd, 1988). Bathymetric
115 surveys from Schneider von Deimling et al. (2010) revealed a rather flat sandy seabed
116 with almost no features, with the exception of cm-sized ripples (McGinnis et al.,
117 2014).

118 The currents of the central North Sea are predominantly driven by the semi-
119 diurnal lunar tide (M_2; Otto et al., 1990). Seasonal stratification starts in April around
120 Julian day 100 (e.g., Meyer et al., 2011). The thermocline has been identified as an
121 important zone for the establishment of primary production and the O_2 maximum
122 layer (see Pingree et al., 1978). In fact, the North Sea deep chlorophyll maximum
123 (DCM) is estimated to account for 58% of the water column primary production and
124 37% of the annual new production for the summer stratified North Sea (Weston et al.,
125 2005). The development of the associated O_2 maximum due to this production is thus
126 important and so far not considered in the overall O_2 balance of the central North Sea.
127
128 ### 2.2 Instrumental setup
129 High resolution (mm scale) turbulent shear and temperature profiles were
130 obtained with a MSS90-L (Sea and Sun Technology, Trappenkamp, Germany)
131 microstructure turbulence profiler. The MSS90-L is a free-falling, loosely-tethered
132 profiler which samples at 1024 Hz with 16 channels and is designed for an optimal

sink rate of 0.5 – 0.6 m s^{-1}. The probe was equipped with two air-foil shear probes, an accelerometer (to correct for probe pitch, roll, and vibration), a fast temperature sensor (FP07, 7–12 ms response time), standard CTD sensors (temperature, pressure, conductivity), and a fast (0.2 s response time) galvanic O_2 sensor (AMT, Analysenmesstechnik GmbH, Rostock, Germany). The absolute O_2 concentrations were calibrated against shipboard CTD O_2 profiles and Winkler titrations on discrete water samples (see below).

Water column hydrodynamics were characterized with the compact benthic Paleoceanography (POZ) lander, which was deployed using a video guided launcher (Pfannkuche and Linke, 2003). The POZ lander recorded 3-dimensional current velocity profiles and acoustic backscatter information throughout the water column using a 300 kHz acoustic Doppler current profiler (ADCP; Workhorse Sentinel, Teledyne RD Instruments, Poway, United States), which sampled every 15 s with a bin size of 0.5 m starting from 2.75 m from the bottom. A conductivity-temperature-depth (CTD) logger (XR-420 CT logger, RBR, Kanata, Canada) recorded temperature, conductivity and pressure (Digiquarz, Paroscientific, Redmond, United States) every 2 s near the seafloor (~0.3 m distance). The POZ lander was also equipped with a Winkler–calibrated O_2 optode sensor (Aanderaa Data Instruments AS, Bergen, Norway), which continuously recorded BBL O_2 concentration at 1 min intervals.

Water column profiles were obtained using a SBE9plus CTD-rosette system (Seabird, Washington, United States). The CTD sampled at 24 Hz and was equipped with standard temperature, conductivity, pressure, O_2 and light transmission sensors. The rosette system mounted 12 10L-Niskin-bottles for discrete water sampling. Each depth (i.e., each Niskin-bottle) was subsampled with three Winkler bottles of known volume (~62 mL on average) right after recovery and the samples were immediately fixed on deck. The samples were then stored in the vessel's cold room and titrated manually within 24 h after the sampling.

2.3 Hydrodynamic data evaluation

The main tidal directions, the major and minor axis of the tidal ellipsoid, were determined by performing a variance analysis on the ADCP velocity time series. The u and v velocities were rotated over a stepwise increasing rotation angle (*r*) as

$u_{rot} = u \cdot cos(-r) - v \cdot sin(-r)$ respectively $v_{rot} = u \cdot sin(-r) - v \cdot cos(-r)$, and the variance computed at each step. The angle at the largest variance represented the main tidal direction. Barotropic and baroclinic flow contributions of tides were separated by least-square fitting the detrended velocity time series to harmonics $u = A \cdot cos(\omega \cdot t + \varphi)$ with A, ω, φ being the amplitude, frequency, and the phase lag, respectively. In the analysis below, the barotropic semi-diurnal principle lunar tide (M_2) and diurnal declination tide (K_1) contributions had frequencies of 1.93227 cycles per day (cpd) and 1.00274 cpd, respectively, and were subtracted from the time series to analyze residual flow. For barotropic contributions, the fit was applied to the depth average of the time series, while baroclinic contributions were obtained by fitting the harmonics to the velocity time series from each 0.5 m ADCP bin. The occurrence of enhanced shear in the stratified water column was investigated by calculating the vertical shear of horizontal velocity, S, from the vertical gradients between adjacent bins of east and north velocity (0.5 m resolution) as $S = \sqrt{(du/dz)^2 + (dv/dz)^2}$. Frequency spectra of the time series of horizontal velocity and vertical shear of horizontal velocity were used to identify the tidal and non-tidal flow components. The spectra were calculated using fast-Fourier transforms combined with a ½-cosine tapper (Hanning window) that was applied to the first and last 10% of the time series data.

Turbulent kinetic energy dissipation rate (ε) was quantified from the airfoil shear readings by integrating shear wavenumber spectra assuming isotropic turbulence (Batchelor, 1953):

$$\varepsilon = 7.5\mu \int_{k_{min}}^{k_{max}} E_{du'/dz}(k)dk \quad (1)$$

where μ is the dynamic viscosity of seawater. Shear spectra $E_{du'/dz}(k)$ were calculated from one-second ensembles (1024 values) and integrated between a lower $k_{\min}$ = 3 cycles per minute (cpm) and an upper wavenumber $k_{\min}$ that varied between 14 cpm and 30 cpm depending on the Kolmogorov wavenumber. Here, a Bartlett window was applied to the whole ensemble prior to spectral decomposition. Loss of variance due to the limited wavenumber band was taken into account by fitting the observed shear spectra to the universal Nasmyth spectrum. Similarly, corrections for the loss of variance due to finite sensor tip of the airfoil probes were applied (see Schafstall et al., 2010). The detection limit, or noise level, of the used profiler for ε

197 was inferred to be 1×10^{-9} W kg^{-1} (Schafstall et al., 2010); the upper detection limit is
198 a function of the shear sensor geometry (up to 10^{-4} W kg^{-1}; Prandke and Stips, 1998).

199 Estimates of the turbulent eddy diffusivities of mass (K_ρ) were obtained from
200 measurements of ε as

$$K_\rho = \gamma\varepsilon/N^2 \quad (2)$$

201 where γ is the mixing efficiency and N^2 the water column stability. This method,
202 proposed by Osborn (1980), approximates K_ρ under the assumption of a local
203 equilibrium of production and dissipation of turbulent kinetic energy. Values for N^2
204 were calculated from temperature, salinity and pressure data using the adiabatic
205 method (Fofonoff, 1985) as $N^2 = -\mathrm{g}(\rho^{-1}\partial\rho/\partial z - g/c^2)$, where ρ, g, and c are the
206 density, the earth's gravitational acceleration and speed of sound, respectively.
207 Mixing efficiency values in stratified waters range from 0.1 to 0.2 (Ivey and
208 Imberger, 1991) and decreases in weakly stratified waters such as within the BBL
209 (Lorke et al., 2008). To account for this decrease, we used the γ and K_ρ
210 parameterization of Shih et al. (2005). Based on the turbulence activity parameter
211 $\varepsilon/\upsilon N^2$, with the kinematic viscosity, ν, the authors found that in energetic regimes,
212 i.e., $\varepsilon/\upsilon N^2 > 100$, the eddy diffusivities are better estimated as $K_\rho = 2\upsilon(\epsilon/\upsilon N^2)^{1/2}$.
213 As horizontal density gradients at the study site were deemed to be small compared to
214 vertical gradients (see Discussion), we equated diapycnal eddy diffusivities with
215 vertical diffusivities (i.e., $K_\rho = K_z$).

216 To obtain representative mean turbulent eddy diffusivities, the data were
217 evaluated in ensembles of three to four consecutive profiles and averaged in depth and
218 time to reduce uncertainties due to the patchiness of turbulence, temporal fluctuation
219 of N^2, as well as temporal γ variations (see Smyth et al., 2001). As proposed by
220 Ferrari and Polzin (2005), the level of uncertainty of the averaged K_z can be
221 quantified as:

$$\Delta K_z = K_z \left[\left(\frac{\Delta\gamma}{\gamma}\right)^2 + \left(\frac{\Delta\varepsilon}{\varepsilon}\right)^2 + \left(\frac{\Delta N^2}{N^2}\right)^2 \right]^{1/2} \quad (3)$$

222 with Δ being the absolute uncertainty of the various average terms. Here, the
223 uncertainties are evaluated in the region of strong vertical O_2 gradients and in 2 m
224 depth bins. The absolute uncertainty for $\Delta\gamma$ was assumed to be 0.04 (see St. Laurent
225 and Schmitt, 1999). The absolute uncertainty on N^2 (ΔN^2) was determined by the

standard error over the 2 m average, computed as the standard deviation divided by the square root of the number of estimates. Finally, the statistical uncertainty of ε for each bin was calculated using a bootstrap method (10^4 resamples) (Efron, 1979).

The vertical O_2 fluxes F_θ were then obtained from K_z and the O_2 concentration gradients $\partial[O_2]/\partial z$ as

$$F_\theta = K_z \frac{\partial [O_2]}{\partial z} \tag{4}$$

Accordingly, the uncertainty of averaged turbulent O_2 fluxes were given by:

$$\Delta F_\theta = F_\theta \left[\left(\frac{\Delta K_z}{K_z} \right)^2 + \left(\frac{\Delta \partial_z [O_2]}{\partial_z [O_2]} \right)^2 \right]^{1/2} \tag{5}$$

where $\Delta \partial_z [O_2]$ denotes the standard error of mean vertical gradients of O_2 concentrations. It should be noted that the analysis did not include biases or uncertainties due to measurement errors.

3 Results

During the three-day observational period (8 – 11 August 2009) we collected 39 high-resolution MSS profiles in sets of three to five profiles that were collected consecutively at 5 – 10 min intervals. Most of the profiles were collected either in the evening (profiles 1 – 8, 26 – 28, 36 – 39) or at night (9 – 15, 29 – 35) with the remaining profiles acquired in the morning (6 to 9 AM). One shipboard CTD profile was performed prior to the actual MSS profiles to provide hydrographic information, the water turbidity and O_2 concentrations, as well as discrete water samples for subsequent onboard Winkler titrations. Hydroacoustic water column current measurements were carried out continuously throughout the observational period. The following results are structured to first present a characterization of the site's physical settings and turbulence drivers, followed by the O_2 fluxes and O_2 BBL budget.

3.1 Water column structure

The ~70 m deep water column was characterized by a stable, well-defined four-layer temperature structure (Fig. 2a). A well-mixed surface boundary layer (SBL) and bottom boundary layer (BBL), 15 m and 30 m thick, respectively, were separated by a weakly-stratified transition layer (15 – 25 m depth) and a strongly stratified interior layer (25 – 40 m depth). The stratified interior layer was

characterized by two very steep thermoclines situated in the upper (27 – 30 m depth) and lower (36 – 39 m depth) region of the layer, with vertical temperature gradients of up to 4°C m^{-1}. The average salinity was 35.08 with little variation throughout the water column (35.04 – 35.1). The light transmission profile from the ship CTD ranged from 89% to 96% (Fig. 2b). The most turbid layer (89%) was observed at the lower boundary of the interior layer (at 40 m depth) suggesting the presence of the deep chlorophyll maximum, phytoplankton, zooplankton and suspended particles.

The O_2 profiles were generally characterized by near saturation in the SBL and transition layers, with O_2 concentrations in the 238 – 243 µmol kg^{-1} range, and undersaturated (~80%) in the BBL, where the O_2 concentration was ~243 µmol kg^{-1} (Fig. 2c,d). The stratified interior was oversaturated by up to 115%, with a well-established O_2 maximum at ~39 m depth with concentrations up to ~315 µmol kg^{-1}. Below that maximum, at the thermocline-BBL interface, we observed a 2 – 3 m thick steep oxycline, with an O_2 gradient of 34 µmol kg^{-1} m^{-1} with exhibited limited day – night, depth and thickness variability. With this in mind, we wish to resolve the O_2 flux into the BBL associated with the oxycline.

3.2 Hydrodynamics

The POZ lander hydrostatic pressure dataset revealed that the tidal water level ranged from 0.6 to 0.9 m (Fig. 3a). Variance analysis on the ADCP velocity data identified the major and minor axis of the tidal ellipsoid components to occur at 45° and 135° from true north, respectively. Along these axes, the current amplitudes were 0.21 m s^{-1} and 0.04 m s^{-1}, indicating a narrow tidal current ellipsoid, as reported by Otto et al. (1990). The site was characterized by a negative tide polarity (anti-cyclonic) for the semi-diurnal tides. A dominance of the barotropic M_2 current amplitude at all depths was also clearly observed in the velocity time series (Fig. 3b, c) and the harmonic analyses. East (zonal) and north (meridional) barotropic M_2-current amplitudes were 0.12 m s^{-1} and 0.17 m s^{-1}, respectively, while K_1-current amplitudes were only 0.005 m s^{-1} and 0.03 m s^{-1}.

Although the limited length of the ADCP velocity time series did not allow for full separation of the M_2 and *f* frequencies, the spectral density functions indicated maximum energy at frequencies of about the semi-diurnal tide. This maximum varied little with depth indicating barotropic M_2 motions. Superimposed on those barotropic

currents, we observed the presence of baroclinic velocity contributions (Fig. 3b, c). Additionally, near-inertial motions were also observed.

The occurrence of near-inertial motions was most pronounced in the thermocline (32 – 39 m; Fig. 3e). Lower but still elevated energy densities at the near-inertial band were also found in the SBL and BBL. Moreover, the near-inertial currents exhibited a distinct 180° phase shift between the SBL and the thermocline as well as between the thermocline and the BBL, suggesting a second vertical mode nature of these fluctuations. Average amplitudes of the near-inertial fluctuations in the thermocline obtained from least-square fitting were 0.11 m s^{-1}. In the BBL and SBL, average amplitudes were reduced to 0.06 m s^{-1} and 0.04 m s^{-1}, respectively, suggesting that *f* oscillations might account for enhanced shear in the thermocline.

Enhanced vertical shear of horizontal velocity was found at the interior – transition layer as well as at the interior – BBL interfacial regions (Fig. 3d). As indicated by the spectral density function of the shear time series from the interior interfacial layers (SI Fig. 1), the shear exhibited near-inertial frequencies (1.6722 cpd), and resulted from the baroclinic near-inertial wave. The high vertical resolution (0.5 m) of our velocity data allowed the resolution of the interfacial shear layers, which were typically 2 to 3 m thick with elevated values of up to 0.05 s^{-1}. Comparisons with CTD data showed that they are collocated with the two enhanced temperature gradients layers in the thermocline (27 – 30 m and 36 – 39 m depth; Fig. 2a).

The dissipation rates (ε) of turbulent kinetic energy (TKE) determined from microstructure shear probes were particularly low ($2 – 5 \times 10^{-9}$ W kg^{-1}) but above the MSS detection limit in the center of the stratified interior. However, TKE increased to 5×10^{-9} W kg^{-1} and 2×10^{-8} W kg^{-1} at the upper and lower interior layer limits, respectively (Fig. 4a). These coincided with the depth range of the interfacial shear layers (Fig. 3d) at the strong temperature gradients (Fig. 2a) and resulting water column stability maxima ($\sim 1 \times 10^{-3}$ s^{-2}).

Bin-averaged values of K_z varied by a factor of 5, ranging from 6×10^{-7} m^2 s^{-1} in the central interior to 3×10^{-6} m^2 s^{-1} in the lower region of the transition layer (Fig. 4b). In the upper interface (thermocline – transition layer), where ε was elevated with respect to the central interior but reduced compared to the lower interfacial layer,

stronger stratification (i.e., larger N^2 values up to 10^{-3} s^{-2}) reduced the eddy diffusivities. At the interior-BBL, higher K_z values (~2×10^{-5} m^2 s^{-1}) resulted from increased turbulence and weaker stratification. This enhanced turbulent transport was located where the vertical O_2 gradient was the strongest (Fig. 2d).

3.3 Oxygen fluxes and budget

With the fast responding AMT galvanic O_2 sensor and rapid sampling rate, we were able to resolve the O_2 gradient with a very high precision. Figure 4c shows the 2 m bin average O_2 fluxes for the interior together with the averages from each ensemble. Small O_2 fluxes (~1 mmol m^{-2} d^{-1}) were estimated for the center and upper region of the interior; this suggested that relatively little O_2 is transported upward from the O_2 maximum to the rest of the interior. In contrast, a substantial O_2 flux ranging from 9 – 134 mmol m^{-2} d^{-1} (average of 54 mmol m^{-2} d^{-1}) was identified from the lower thermocline towards the BBL. The confidence interval associated with the uncertainties of the O_2 flux estimates was 18 – 74 mmol m^{-2} d^{-1}. Although the O_2 fluxes to the BBL water from the thermocline were variable in magnitude (Fig. 4c), and the measurements limited to the observational period (Fig. 3), their magnitude nevertheless suggests an important, yet overlooked, O_2 pathway.

We performed a simple 1-D BBL mass balance to investigate the relevance to the local O_2 balance during our observational period. Here, we defined the apparent (measured) O_2 loss rate in the BBL $\partial[O_2]/\partial t$ as the consequence of O_2 replenishment from F_θ and the O_2 utilization via sediment O_2 uptake rate (*SUR*) and water column organic matter respiration (*R*) expressed as

$$\frac{\partial[O_2]}{\partial t}\frac{V}{A} = |F_\theta| - |SUR| - |R| \quad \{mmol\ m^{-2}\ d^{-1}\} \tag{6}$$

The mass balance was constrained to the (assumed) well-mixed 35 m deep BBL section of area, A = 1 m^2 with a volume, V = 35 m^3. We further assumed negligible horizontal O_2 gradients (as observed from the CTD casts), and thus a net zero horizontal O_2 advective transport.

The average *SUR* for the same time period and location obtained from parallel eddy correlation measurements, was ~-10 mmol m^{-2} d^{-1} (McGinnis et al., 2014). The *SUR* was consistent with the average *SUR* at Oyster Grounds reported by Neubacher et al. (2011), -9.8 mmol m^{-2} d^{-1}, as well as with modeled *SUR*s at the same site

(average -8.6 mmol m^{-2} d^{-1}; Meire et al., 2013). The apparent BBL O_2 loss of -0.42 µmol kg^{-1} d^{-1} was determined from the POZ lander O_2 optode time series (Fig. 5a) over 52 hours, (R^2=0.60). Though limited to our short observational period, the vertically integrated apparent BBL O_2 loss was about -15 mmol m^{-2} d^{-1} and thus within 2% of the nearby North Dogger average presented by Greenwood et al. (2010). Based on Eq. (6) and using the observed BBL O_2 loss rate, F_θ and *SUR*, the water column respiration, *R* was calculated to be ~-60 mmol m^{-2} d^{-1}. This implies that without the O_2 replenishment, the apparent BBL O_2 loss would be ~-2 µmol kg^{-1} d^{-1} and thus four times higher than observed. Our results indicated that the total respiration in the bottom water was therefore ~-70 mmol m^{-2} d^{-1} (*SUR* + *R*), with about 14% of the organic carbon mineralization occurring at the sediment and 86% in the BBL.

4 Discussion

During our three-day observational period, we found that the baroclinic near-inertial wave in the interior was the main contributor to the detected enhanced shear (Fig. 3d) and the observed elevated vertical O_2 flux to the BBL (Fig. 6). As near-inertial waves decay after a few weeks, it should be noted that we observed a rather special situation, and that vertical O_2 fluxes will not likely be as highly elevated during periods when near-inertial waves are not present.

Within this context, we will: 1) discuss the turbulent mechanisms leading to these thermocline O_2 fluxes and those promoting the formation of the O_2 maximum zone in terms of primary productivity; 2) discuss the implication for the local O_2 BBL dynamics and carbon budget; 3) speculate on factors that can ultimately influence O_2 depletion in the North Sea and other seasonally stratified shelf seas.

4.1 Thermocline mixing

The expansive North Sea thermocline ($1 – 5\ 10^5$ km^2; Meyer et al., 2011) has been regarded as being in a state of marginal stability, where additional sources of shear could lead to increased thermocline mixing (e.g., van Haren et al., 1999). Itsweire et al. (1989) showed that layers of strong shear are likely to be found where strong stratification occurs. In general, away from varying topography, the major sources of shear in the thermocline are considered to be internal tides and near-inertial

384 oscillations (see Rippeth, 2005). Sharples et al. (2007) demonstrated that internal
385 tidally-driven thermocline mixing also enhanced diapycnal nutrient fluxes, the overall
386 productivity in the thermocline, as well as the associated carbon export to the BBL.

387 The occurrence of near-inertial oscillations in shelf seas during the stratified
388 season has been reported in several studies from the North Sea (van Haren et al.,
389 1999; Knight et al., 2002) as well as in other shelf seas (e.g., Rippeth et al., 2002;
390 McKinnon and Gregg, 2005). During the presence of baroclinic inertial waves in the
391 water column, periods of enhanced shear taking the form of shear spikes occur
392 approximately every inertial period and in bursts lasting several days have been
393 observed in the western Irish Sea (Rippeth et al., 2009), the Celtic Sea (Palmer et al.,
394 2008) and the northern North Sea (Burchard and Rippeth, 2009).

395 While we mainly attributed the observed enhanced turbulent mixing to the
396 occurrence of a near-inertial wave, the site's physical setting has further implications
397 for mixing processes in the thermocline. In the northern hemisphere, sites with anti-
398 cyclonic tides, such as Tommeliten, are often characterized by an increased vertical
399 extension of the BBL, and higher BBL dissipation rates than comparable cyclonic
400 sites (see Simpson and Tinker, 2009). As a result of this enhanced BBL thickness, we
401 observed sporadically elevated thermocline turbulence resulting from tidal-driven
402 bottom turbulence propagating vertically to the thermocline (Fig. 5b). A study by
403 Burchard and Rippeth (2009) also reported that short lived thermocline shear spikes
404 can arise due to the alignment of the surface wind stress, bulk shear, and bed stress
405 vectors in the presence of baroclinic near-inertial motions and barotropic tidal
406 currents. These mechanisms are stronger with anti-cyclonic tides. Although all the
407 features required for shear spike generation were present during the observational
408 period, the two-layer mechanism described by these authors would require a more
409 complex water column structure to be applicable to the Tommeliten site.

410 The site's water column structure clearly showed the occurrence of a 10 m
411 thick transition layer (Fig. 2a). This layer represents the region of the water column
412 where mixing turns from elevated in the SBL to strongly reduce in the interior
413 (Ferrari and Boccaletti, 2004). The transition layer represents an obligate pathway for
414 solute and heat exchange between SBL and the interior (Ferrari and Boccaletti, 2004;
415 Rhein et al., 2010) and has also been reported to be a region of enhanced shear and
416 near-inertial wave activity (Dohan and Davis, 2011). Although the presented data did

not allow a quantification of the O_2 exchange across the transition layer, such contribution might be considerable and thus highly relevant for the cycling of O_2 and CO_2 in the upper water column, which in turn could have direct biological implications.

4.2 BBL O_2 dynamics

Ultimately, observed O_2 depletion in the BBL of the central North Sea depends on the supply of organic matter, the rate of carbon mineralization, and the flux of O_2 to the bottom water either from horizontal advection or turbulent vertical transport. Our study investigated the significance of turbulent vertical O_2 fluxes to the BBL, which has been previously overlooked in shelf sea carbon balances. Studies focusing on O_2 replenishment in the BBL through the thermocline are limited to freshwater systems (e.g. Bouffard et al., 2013; Kreling et al., 2014). In a large stratified water body such as Lake Erie, O_2 transport from the thermocline to the hypolimnion was found to be substantial, with a magnitude comparable to ~18% of the hypolimnetic O_2 utilization rate over the whole stratification period (Bouffard et al., 2013).

Horizontal O_2 gradients and associated horizontal advective O_2 fluxes were not quantified in this study. Our data does, however, suggest that such fluxes would not significantly contribute to the O_2 balance at the Tommeliten site. BBL O_2 concentration time series (Fig. 5a) did not show any variability at the tidal and or inertial frequencies, implying that horizontal O_2 gradients were small. Additionally, mean currents in the BBL were also small (~2 cm s^{-1}) compared to the tidal amplitudes. This, in conjunction with weak horizontal O_2 gradients, suggests that horizontal advective O_2 fluxes during our observational period are negligible compared to the turbulent O_2 flux from the thermocline.

Based on the above, we can argue that the O_2 dynamics during the stratified period are more complicated than previously regarded. To maintain an excess of O_2 in the thermocline, primary producers require adequate nutrient entrainment from the bottom water to fuel potential new production. The resulting increase in (new) productivity and subsequent export to the bottom water could therefore boost the carbon turnover estimates substantially. Using a 1:1 O_2 utilization – carbon re-mineralization (see Canfield, 1993), Greenwood et al. (2010) inferred the average

BBL carbon re-mineralization rate at the nearby North Dogger to be 15 mmol m^{-2} d^{-1}, or 180 mg C m^{-2} d^{-1}. Similar results for a typical NW European shelf sea were obtained via modeling by Sharples (2008), who reported rates ranging from ~35 to ~200 mg m^{-2} d^{-1} for neap and spring tide, respectively. Their study, however, did not include the daily tidal variation, and thus rates could be much higher on shorter timescales.

With the absence of targeted long-term studies focusing on O_2 and carbon dynamics in the thermocline and BBL, we can only speculate on the long-term fate of the BBL O_2 and its replenishment from the thermocline by vertical O_2 fluxes (F_θ). However, it seems possible over that the overall net BBL water column O_2 respiration, R, is higher than previously thought, suggesting a much higher carbon turnover than inferred from the apparent O_2 loss rate. Based on Eq. (6), the BBL carbon re-mineralization (and export to the BBL) would be on the order of nearly 850 mg C m^{-2} d^{-1}, almost a factor of 5 higher than reported by Greenwood et al. (2010). However, the same turbulent transport that supports the O_2 export from the DCM to the BBL also supports BBL nutrient import to the DCM (Fig. 6). The higher import of nutrients to the DCM likely promotes additional primary production and a subsequent increase in organic matter (OM) export to the BBL. In such a scenario, the ephemeral O_2 flux to the BBL presented in this study will be associated with additional OM to the BBL, and therefore lead to a temporary increased re-mineralization that offsets the increased F_θ. While the overall effect is an increase in carbon turnover, this process therefore does not result in any observable change in the decreasing O_2 trend (apparent O_2 loss rate).

4.3 Causes and controls on BBL O_2 depletion

According to Boers (2005), for BBL O_2 to decrease throughout the stratified season, there must be suitable physical conditions, biomass production, nutrient input and continued benthic O_2 uptake. *SUR*, and thus the sediment nutrient release and organic carbon mineralization have been shown to be strongly tidal-driven (McGinnis et al., 2014). Therefore, we briefly discuss the potential tidal impact driving the overall carbon cycling and suggest factors that may promote the development of lower BBL O_2 concentrations during the stratification period.

Tidal forcing on diapycnal constituent fluxes and primary production have been explored by e.g., Sharples et al. (2007, 2008). The authors showed that spring-neap tide drives nutrient fluxes between the BBL and the DCM at the thermocline, as well as the carbon export. Based on our velocity measurements and estimated O_2 fluxes, we can also expect similar patterns corresponding to semidiurnal tidal fluctuations. Blauw et al. (2012) investigated fluctuating phytoplankton concentrations in relation to tidal drivers and found in the southern North Sea that chlorophyll fluctuations correlated with the typical tidal current speed periods, the semidiurnal tidal cycle, in addition to the day-night and spring-neap periods. During most of the year, chlorophyll and suspended particulate matter fluctuated in phase with tidal current speed, and indicated alternating periods of sinking and vertical mixing of algae and suspended matter with tidal cycles. Thus, these results suggest that we can expect the semidiurnal tidal-driven export of carbon and O_2 from the DCM to the BBL, as well as entrainment of nutrients that strongly vary based on a timescale related to the semi-diurnal tidal cycle, in addition to the spring-neap tidal cycles.

The flux of O_2 from the DCM production zone downward to the BBL could set the lower limit of the BBL O_2 concentration, and thus the O_2 depletion level, during the stratification period. If there is little isolation between the zone of production and the zone of mineralization, then the net O_2 production and O_2 utilization would nearly balance. In such case the apparent O_2 loss in the BBL would either be negligible or very small, depending whether the largely particle organic matter driven SUR will be balanced by the ventilation form the thermocline. However, historically decreasing BBL O_2 concentrations within the North Sea (Queste et al., 2013) point to an increasing disconnect between the main O_2 production zone and the mineralization zones. Greenwood et al. (2010) state that stratification is an important factor which determines susceptibility to O_2 depletion, especially in their nearby study site Oyster Grounds.

Surveys on the North Sea have shown that the regions with the lowest BBL O_2 concentrations are generally characterized by the strongest stratification (see Queste et al., 2013), and the lowest reported values (~100 μmol kg^{-1}) were also reported to occur during particularly calm and warm weather (see Boers, 2005; Weston et al., 2008). Strong gradients in the thermocline are suggested to limit the O_2 flux to the

515 BBL (Weston et al., 2008), and point to the potential future O_2 depletion resulting
516 from increasing temperatures leading to both stronger stratification and a longer
517 stratification season (Lowe et al., 2009). However, it could be expected that if O_2
518 fluxes between the DCM and BBL were suppressed, then the upward nutrient fluxes
519 would be similarly suppressed, thus inhibiting primary production and therefore not
520 resulting in observed O_2 deficits.
521
522 **4.4 Biological perspective**

523 The occurrence of stronger stratification might have much larger implications
524 than presently thought, since reduced turbulent mixing will alter algal populations
525 (Hickman et al., 2009), potentially favoring migrating/swimming phytoplankton. An
526 example of these migrating phytoplankton species, armored dinoflagellates, are
527 extensively found in the DCM of the central and northern North Sea during the
528 summer months; their abundance was found to be largely determined by the local
529 hydrodynamic conditions (Reid et al., 1990). In calm conditions, which are typically
530 associated with stronger stratification, there are often blooms of migrating
531 dinoflagellates which have access to the large nutrient pool in the deeper water and
532 can therefore out-compete non-migrating species for both light and nutrients. Stronger
533 turbulent mixing, in contrast, has been suggested to interfere with their swimming
534 abilities and thus favoring other algal species (see Jephson et al., 2012 and references
535 therein).

536 Migration-driven movement of the DCM higher in the thermocline, even by a
537 few meters, means that the O_2 production will be shifted higher in the thermocline.
538 Migrating phytoplankton could therefore access BBL nutrients in this scenario, i.e.,
539 primary production rates would be comparable, but the result would be an evident
540 further decrease in the BBL O_2. For example, assuming our previous values of *SUR*
541 and *R* in Eq. (6), but reducing F_θ by half results in a nearly 3x increase in the apparent
542 O_2 loss rate. Therefore, the combined effects of reduced turbulent O_2 flux and a
543 reduced O_2 gradient at the base of the thermocline, will both further isolate the BBL
544 from this potential O_2 supply while maintaining similar rates of carbon export
545 (settling armored dinoflagellates). We speculate that this mechanism could therefore
546 provide a further loss of O_2 connectivity as the amount of production would remain
547 approximately the same, but the supply of O_2 to the BBL would be substantially

548 reduced. Of course, whether such scenario could be sustained over the whole
549 stratification period is not known and requires further assessment.

550 In the light of climatic changes, studies have suggested that O_2 loss in the
551 North Sea bottom waters would mainly result from a strengthening of the
552 stratification and O_2 solubility reduction with increasingly warmer waters (e.g., Meire
553 et al., 2013). The findings of this study suggest there might be an additional level of
554 complexity based on the interplay between the tidally-driven physics, water column
555 structure, biogeochemical cycling and active phytoplankton migration in the central
556 North Sea. The proposed mechanism could contribute to the observed decreasing O_2
557 levels in the North Sea water column, however, further detailed studies are obviously
558 necessary to validate and fully quantify this effect at the seasonal level.

559

560 **Acknowledgements**

561 We are thankful to the captain and crewmembers of the R/V *Celtic Explorer*
562 for their outstanding collaboration and support during the survey, Uwe Koy and
563 Rudolf Link for their logistic support, and Jens Schafstall, Tim Fischer and Markus
564 Faulhaber for their help in data collection and processing. We are grateful for the
565 technical development and support in deployment of the benthic chamber by Ralf
566 Schwarz, Sergiy Cherednichenko and the ROV Kiel 6000 team. Financial support was
567 provided by the Sonderforschungsbereich (SFB) 754 "Climate – Biogeochemisty in
568 the tropical Ocean", SFB 574 "Volatiles and Fluids in Subduction Zones", and by the
569 Excellence Cluster "Future Ocean" (project 2009/1 CP 0915, LR), supported by the
570 Deutsche Forschungsgemeinschaft (DFG). Additional founding was provided by the
571 National Environmental Research Council (NERC, project NE/J011681/1). The cruise
572 was financed by Wintershall within the Fluid and Gas Seepage in the Southern
573 German North Sea (SDNS) project.

574

References

Batchelor, G. K.: The theory of homogeneous turbulence, Cambridge University Press, Cambridge, 1953.

Best, M. A., Wither, A. W., and Coates, S.: Dissolved oxygen as a physico-chemical supporting element in the Water Framework Directive, Mar. Pollut. Bull., 55, 53–64, doi:10.1016/j.marpolbul.2006.08.037, 2005.

Blauw, A. N., Beninca, E., Laane, R. W. P. M., Greenwood, N., and Huisman, J.: Dancing with the tides: fluctuations of coastal phytoplankton orchestrated by different oscillatory modes of the tidal cycle, Plos One, 7, e49319, doi:10.1371/journal.pone.0049319, 2012.

Boers, M.: Effects of a deep sand extraction pit. Final report of the PUTMOR measurements at the Lowered Dump Site, Rijkswa- terstaat, The Netherlands, RIKZ/2005.001, 87, 2005.

Bouffard, D., Ackerman, J. D., and Boegman, L.: Factors affecting the development and dynamics of hypoxia in a large shallow stratified lake: hourly to seasonal patterns, Water Resour. Res., 49, 2380–2394, doi:10.1002/wrcr.20241, 2013.

Brandt, P., Bange, H., Banyte, D., Dengler, M., Didwischus, S-H., Fischer, T., Greatbatch, R., Hahn, J., Kanzow, T., Karstensen, J., Körtzinger, A., Krahmann, G., Schmidtko, S., Stramma, L., Tanhua T., and Visbeck, M.: On the role of circulation and mixing in the ventilation of oxygen minimum zones with a focus on the eastern tropical North Atlantic, Biogeosciences, 12, 489–512, doi:10.5194/bg-12-489-2015, 2015.

Burchard, H., and Rippeth, T. P.: Generation of bulk shear spikes in shallow stratified tidal seas, J. Phys. Oceanogr., 39, 969–985, doi:10.1175/2008JPO4074.1, 2009.

Canfield, D. E.: Organic matter oxidation in marine sediments, in: Interactions of C, N, P and S biogeochemical cycles and global change, edited by: Wollast, R., Mackenzie, F. T., and Chou, L., Springer, Berlin, 333–363, 1993.

Chan, F., Barth, J. A., Lubchenco, J., Kirincich, A., Weeks, H., Peterson, W. T., and Menge, B. A.: Emergence of anoxia in the California current large marine ecosystem, Science, 319, 920–920, doi:10.1126/Science.1149016, 2008.

605 Crawford, W. R., and Pena, M. A.: Declining oxygen on the British Columbia
606 continental shelf, Atmos. Ocean., 51, 88–103, doi:10.1080/07055900.2012.753028,
607 2013.

608 Diaz, R. J.: Overview of hypoxia around the world, J. Environ. Qual., 30, 275–281,
609 doi:10.2134/jeq2001.302275x, 2001.

610 Diaz, R. J., and Rosenberg, R. : Spreading dead zones and consequences for marine
611 ecosystems, Science, 321, 926–929, doi:10.1126/Science.1156401, 2008.

612 Dohan, K, and Davis, R. E.: Mixing in the transition layer during two storm events, J.
613 Phys. Oceanogr., 41, 42–66, doi:10.1175/2010jpo4253.1, 2011.

614 Efron, B.: 1977 Rietz lecture - bootstrap methods - another look at the jackknife, Ann.
615 Stat., 7, 1–26, 1979.

616 Ferrari, R., and Boccaletti, G.: Eddy-mixed layer interactions in the ocean,
617 Oceanography, 17, 12–21, doi:10.5670/oceanog.2004.26. 2004.

618 Ferrari, R., and Polzin, K. L.: Finescale structure of the T-S relation in the eastern
619 North Atlantic, J. Phys. Oceanogr., 35, 1437–1454, doi:10.1175/JPO2763.1, 2005.

620 Fischer, T., Banyte, D., Brandt, P., Dengler, M., Krahmann, G., Tanhua, T., and
621 Visbeck, M.: Diapycnal oxygen supply to the tropical North Atlantic oxygen
622 minimum zone, Biogeosciences, 10, 5079–5093, doi:10.5194/bg-10-5079-2013, 2013.

623 Fofonoff, N. P.: Physical properties of seawater: A new salinity scale and equation of
624 state for seawater, J. Geophys. Res., 90, 3332–3342, doi:10.1029/Jc090ic02p03332,
625 1985.

626 Glud, R. N.: Oxygen dynamics of marine sediments, Mar. Biol. Res., 4, 243–289,
627 doi:10.1080/17451000801888726, 2008.

628 Grantham, B. A., Chan, F., Nielsen, K. J., Fox, D. S., Barth, J. A., Huyer, A.,
629 Lubchenco, J., and Menge, B. A.: Upwelling-driven nearshore hypoxia signals
630 ecosystem and oceanographic changes in the northeast Pacific, Nature, 429, 749–754,
631 doi:10.1038/Nature02605, 2004.

632 Greenwood, N., Parker, E. R., Fernand, L., Sivyer, D. B., Weston, K., Painting, S. J.,
633 Kroger, S., Forster, R. M., Lees, H. E., Mills, D. K., and Laane, R. W. P. M.:
634 Detection of low bottom water oxygen concentrations in the North Sea; implications

635 for monitoring and assessment of ecosystem health, Biogeosciences, 7, 1357–1373,
636 doi:10.5194/bg-7-1357-2010, 2010.

637 Hickman, A. E., Holligan, P. M., Moore, C. M., Sharples, J., Krivtsov, V., and
638 Palmer, M. R.: Distribution and chromatic adaptation of phytoplankton within a shelf
639 sea thermocline, Limnol. Oceanogr., 54, 525–536, doi:10.4319/lo.2009.54.2.0525,
640 2009.

641 Hovland, M., and Judd, A.: Seabed pockmarks and seepage: Impact on geology,
642 biology and the marine environment, Graham and Trotman, London, 1988.

643 Itsweire, E. C., Osborn, T. R., and Stanton, T. P.: Horizontal distribution and
644 characteristics of shear layers in the seasonal thermocline, J. Phys. Oceanogr., 19,
645 302–320, doi:10.1175/1520-0485(1989)019<0301:HDACOS>2.0.CO;2, 1989.

646 Ivey, G. N., and Imberger, J.: On the nature of turbulence in a stratified fluid, Part I:
647 The energetics of mixing, J. Phys. Oceanogr., 21, 650–658, doi:10.1175/1520-
648 0485(1991) 021<0650:OTNOTI>2.0.CO;2, 1991.

649 Jephson, T., Carlsson, P., and Fagerberg, T.: Dominant impact of water exchange and
650 disruption of stratification on dinoflagellate vertical distribution, Estuarine, Coastal
651 Shelf Sci., 112, 198–206, doi:10.1016/j.ecss.2012.07.020, 2012.

652 Jørgensen, B. B., and Revsbech, N. P.: Diffusive boundary layers and the oxygen
653 uptake of sediments and detritus, Limnol. Oceanogr., 30, 111–122,
654 doi:10.4319/lo.1985.30.1.0111, 1985.

655 Kemp, W. M., Testa, J. M., Conley, D. J., Gilbert, D., and Hagy, J. D.: Temporal
656 responses of coastal hypoxia to nutrient loading and physical controls,
657 Biogeosciences, 6, 2985–3008, doi:10.5194/bg-6-2985-2009, 2009.

658 Knight, P. J., Howarth, M. J., and Rippeth, T. P.: Inertial currents in the northern
659 North Sea, J. Sea Research, 47, 269–284, doi:10.1016/S1385-1101(02)00122-3, 2002.

660 Kreling, J., Bravidor, J., McGinnis, D. F., Koschorreck, M., and Lorke, A.: Physical
661 controls of oxygen fluxes at pelagic and benthic oxyclines in a lake, Limnol.
662 Oceanogr., 59, 1637–1650, doi:10.4319/lo.2014.59.5.1637, 2014.

663 Lorke, A., Umlauf, L., and Mohrholz, V.: Stratification and mixing on sloping
664 boundaries, Geophys. Res. Lett., 35, L14610, doi:10.1029/2008GL034607, 2008.

Lowe, J. A., Howard, T. P., Pardaens, A., Tinker, J., Holt, J., Wakelin, S., Milne, G., Leake, J., Wolf, J., Horsburgh, K., Reeder, T., Jenkins, G., Ridley, J., Dye, S., and Bradley, S.: UK Climate Projections science report: Marine and coastal projections. Met Office Hadley Centre, available at: http://ukclimateprojections.metoffice.gov.uk/22530, 2009.

MacKinnon, J. A., and Gregg, M. C.: Near-inertial waves on the New England shelf: The role of evolving stratification, turbulent dissipation, and bottom drag, J. Phys. Oceanogr., 35, 2408–2424, doi:10.1175/JPO2822.1, 2005.

McGinnis, D. F., Sommer, S., Lorke, A., Glud, R. N., and Linke, P.: Quantifying tidally driven benthic oxygen exchange across permeable sediments: An aquatic eddy correlation study, J. Geophys. Res.: Oceans, 119, 6918–6932, doi:10.1002/2014JC010303, 2014.

Meire, L., Soetaert, K. E. R., and Meysman, F. J. R.: Impact of global change on coastal oxygen dynamics and risk of hypoxia, Biogeosciences, 10, 2633–2653, doi:10.5194/bg-10-2633-2013, 2013.

Meyer, E. M. I., Pohlmann, T., and Wiesse, R.: Thermodynamic variability and change in the North Sea (1948-2007) derived from a multidecadal hindcast, J. Mar. Syst., 86, 35–44, doi:10.1016/j.jmarsys.2011.02.001, 2011.

Neubacher, E. C., Parker, R. E., and Trimmer, M.: Short-term hypoxia alters the balance of the nitrogen cycle in coastal sediments, Limnol. Oceanogr., 56, 651–665, doi:10.4319/lo.2011.56.2.0651, 2011.

North Sea Task Force: North Sea Quality Status Report, Report No.: 1 872349 05 6, London: Oslo and Paris Commissions, 1993.

Osborn, T. R.; Estimates of the local rate of vertical diffusion from dissipation measurements, J. Phys. Oceanogr., 10, 83–89, doi:10.1175/1520-0485(1980)010<0083: EOTLRO>2.0.CO;2, 1980.

OSPAR (Oslo-Paris convention for the protection of the marine environment of the North-East Atlantic): EcoQO Handbook—Handbook for the application of ecological quality objectives in the North Sea, Report No.: 978-1-905859-46-7, 2nd edn., OSPAR Biodiversity Series 2009/307, available at http://www.ospar.org/v_publications/browse.asp, 2009.

OSPAR: Quality Status Report 2010, Report No: 978-1-906840-44-0, OSPAR Commission, London, available at http://qsr2010.ospar.org/en/index.html, 2010.

Otto, L., Zimmerman, J. T. F., Furnes, G. K., Mork, M., Saetre, R., and Becker, G.: Review of the physical oceanography of the North Sea, Ned. J. Sea Res., 26, 161–238, doi:10.1016/0077-7579(90)90090-4, 1990.

Palmer, M. R., Rippeth, T. P., and Simpson, J. H.: An investigation of internal mixing in a seasonally stratified shelf sea, J. Geophys. Res., 113, C12005, doi:10.1029/2007JC004531, 2008.

Pfannkuche, O., Linke, P.: GEOMAR landers as long-term deep-sea observatories, Sea Technol. 44, 50–55, 2003.

Pingree, R. D., Holligan, P. M., and Mardell, G. T.: The effect of vertical stability on phytoplankton distributions in the summer on the Northwest European Shelf, Deep Sea Res., 25, 1011–1028, doi:10.1016/0146-6291(78)90584-2, 1978.

Prandke, H., and Stips, A.: Test measurements with an operational microstructure-turbulence profiler: Detection limit of dissipation rates, Aquat. Sci., 60, 191–209, doi:10.1007/s000270050036, 1998.

Queste, B.Y., Fernand, L., Jickells, T. D., and Heywood, K. J.: Spatial extent and historical context of North Sea oxygen depletion in August 2010, Biogeochemistry, 113, 53–68, doi:10.1007%2Fs10533-012-9729-9, 2013.

Radach, G. and Lenhart, H. J.: Nutrient dynamics in the North Sea: Fluxes and budgets in the water column derived from ERSEM, Neth. J. Sea Res., 33, 301–335, doi:10.1016/0077-7579(95)90051-9, 1995

Reid, P. C., Lancelot, C., Gieskes, W. W. C., Hagmeier, E., and Weichart, G.: Phytoplankton of the North Sea and its dynamics - a review, Neth. J. Sea Res., 26, 295–331, doi:10.1016/0077-7579(90)90094-W, 1990.

Rhein, M., Dengler, M., Sültenfuß, J., Hummels, R., Hüttl-Kabus, S., and Bourles, B.: Upwelling and associated heat flux in the equatorial Atlantic inferred from helium isotope disequilibrium, J. Geophys. Res., 115, C08021, doi:10.1029/2009JC005772, 2010.

Rippeth, T. P.: Mixing in seasonally stratified shelf seas: A shifting paradigm, Phil. Trans. R. Soc. A, 363, 2837–2854, doi:10.1098/rsta.2005.1662, 2005.

727 Rippeth, T. P., Simpson, J. H., Player, R., and Garcia, M. C.: Current oscillations in
728 the diurnal-inertial band on the Catalonian Shelf in spring, Cont. Shelf Res., 22, 247–
729 265, doi:10.1016/S0278-4343(01)00056-5, 2002.

730 Rippeth, T. P., Wiles, P., Palmer, M. R., Sharples, J., and Tweddle, J.: The diapcynal
731 nutrient flux and shear-induced diapcynal mixing in the seasonally stratified western
732 Irish Sea, Cont. Shelf Res., 29, 1580–1587, doi:10.1016/j.csr.2009.04.009, 2009.

733 Schafstall, J., Dengler, M., Brandt, P., and Bange, H.: Tidal-induced mixing and
734 diapycnal nutrient fluxes in the Mauritanian upwelling region, J. Geophys. Res.:
735 Oceans, 115, C10014, doi:10.1029/2009jc005940, 2010.

736 Sharples, J.: Potential impacts of the spring-neap tidal cycle on shelf sea primary
737 production, J. Plankton Res., 30, 183–197, doi: 10.1093/plankt/fbm088, 2008.

738 Sharples, J., Moore, C. M., Rippeth, T. P., Holligan, P. M., Hydes, D. J., Fisher, N.
739 R., and Simpson, J. H.: Phytoplankton distribution and survival in the thermocline,
740 Limnol. Oceanogr., 46, 486–496, doi:10.4319/lo.2001.46.3.0486, 2001.

741 Sharples, J., Tweddle, J. F., Green, J. A. M., Palmer, M. R., Kim, Y. N., Hickman, A.
742 E. Holligan, P. M., Moore, C. M., Rippeth, T. P., Simpson, J. H., and Krivtsov, V.:
743 Spring-neap modulation of internal tide mixing and vertical nitrate fluxes at a shelf
744 edge in summer, Limnol. Oceanogr., 52, 1735–1747, doi: 10.4319/lo.2007.52.5.1735,
745 2007.

746 Schneider von Deimling, J., Greinert, J., Chapman, N. R., Rabbel, W., and Linke, P.:
747 Acoustic imaging of natural gas bubble ebullition in the North Sea: Sensing the
748 temporal, spatial and activity variability, Limnol. Oceanogr.: Methods, 8, 155–171,
749 doi:10.4319/ lom.2010.8.155, 2010.

750 Shih, L. H., Koseff, J. R., Ivey, G. N., and Ferziger, J. H.: Parameterization of
751 turbulent fluxes and scales using homogeneous sheared stably stratified turbulence
752 simulations, J. Fluid Mech., 525, 193–214, doi:10.1017/S0022112004002587, 2005.

753 Simpson, J. H., and Tinker, J. P.: A test of the influence of tidal stream polarity on the
754 structure of turbulent dissipation, Cont. Shelf Res., 29, 320–332, doi:10.1016/
755 j.csr.2007.05.013, 2009.

756 Smyth, W. D., Moum, J. N., and Caldwell, D. R.: The efficiency of mixing in
757 turbulent patches: inferences from direct simulations and microstructure observations,

J. Phys. Oceanogr., 31, 1969–1992, doi:10.1175/1520-0485(2001)031<1969:TEOMIT>2.0.CO;2, 2001.

St. Laurent, L., and Schmitt, R. W.: The contribution of salt fingers to vertical mixing in the North Atlantic Tracer Release Experiment, J. Phys. Oceanogr., 29, 1404–1424, 1999.

Thomas, H., Bozec, Y., de Baar, H. J. W., Elkalay, K., Frankignoulle, M., Schiettecatte, L.-S., Kattner, G., and Borges, A. V.: The carbon budget of the North Sea, Biogeosciences, 2, 87–96, doi:10.5194/bg-2-87-2005, 2005.

van Haren, H., Mass, L., Zimmerman, J. T. R., Ridderinkhof, H., and Malschaert, H.: Strong inertial currents and marginal internal wave stability in the central North Sea, Geophys. Res. Lett., 26, 2993–2996, doi:10.1029/1999GL002352, 1999.

Vaquer-Sunyer, R., and Duarte, C. M.: Thresholds of hypoxia for marine biodiversity, P. Natl. Acad. Sci. USA., 105, 15452–15457, doi:10.1073/pnas.0803833105, 2008.

Wanninkhof, R.: Relationship between wind speed and gas exchange over the ocean, J. Geophys. Res.: Oceans, 97, 7373–7382, doi:10.1029/92jc00188, 1992

Weston, K., Fernand, L., Mills, D. K., Delahunty, R., and Brown, J.: Primary production in the deep chlorophyll maximum of the central North Sea, J. Plankton Res., 27, 909–922, doi:10.1093/plankt/fbi064, 2005.

Weston, K., Greenwood, N., Fernand, L., Pearce, D. J., and Sivyer, D. B.: Environmental controls on phytoplankton community composition in the Thames plume, U.K. J. Sea Res., 60, 246–254, doi:10.1016/j.seares.2008.09.003, 2008.

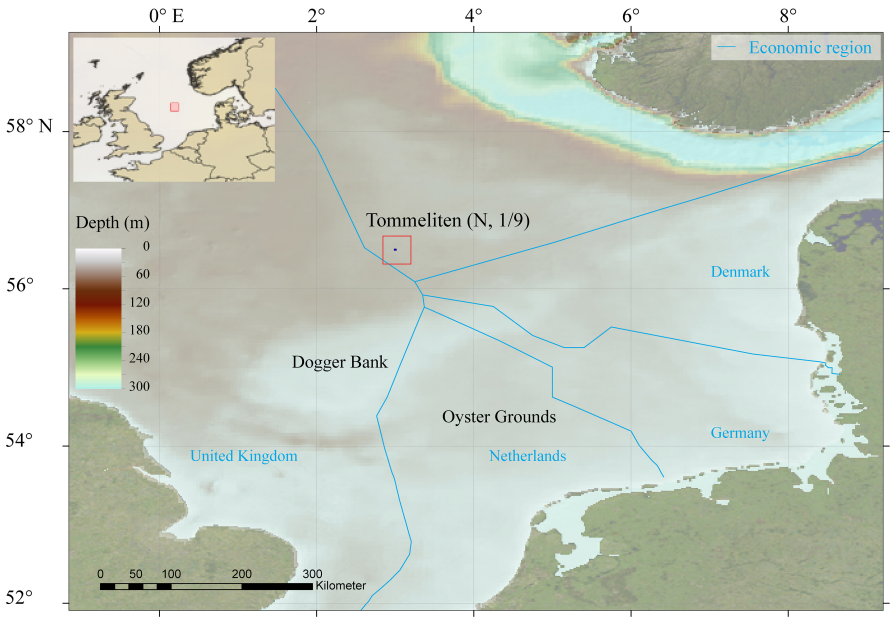

780
781

782 Figure 1. Map of the North Sea indicating the water depths and location of the
783 Tommeliten site as well as the borders of the economic regions of the surrounding
784 European countries.

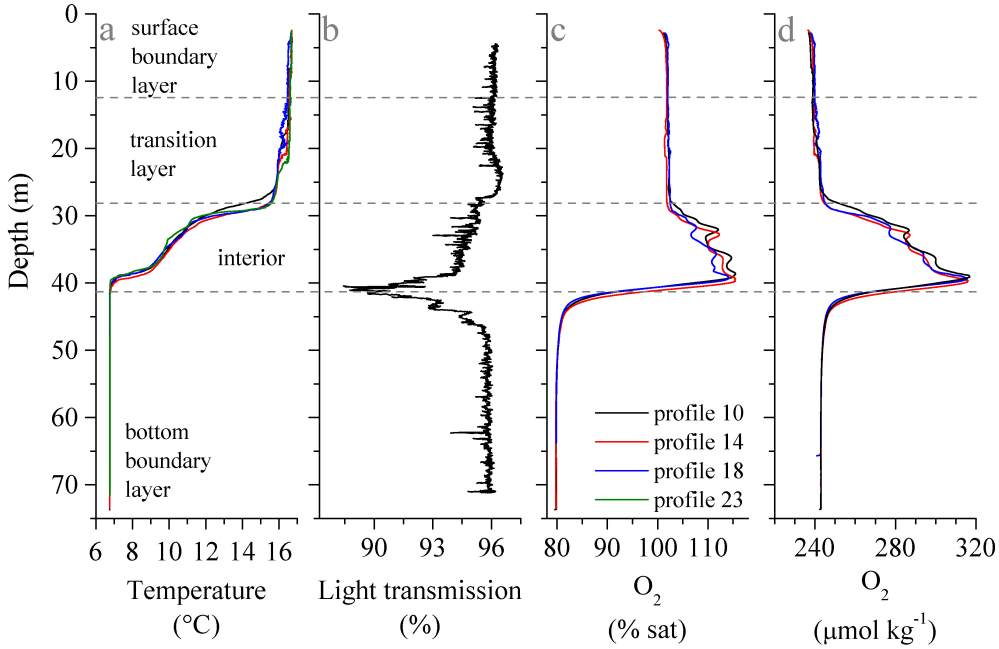

785

786

787 Figure 2. Selected water column profiles based on based on high-resolution MSS
788 profiles (a, c, d) and ship CTD profile (b). (a) Potential temperature profiles. Water
789 column layers were identified based on the temperature profiles. A 0.2°C and 1.5°C
790 decrease from the surface boundary layer average temperature (3–6 m depth) was
791 used determine the depth of the surface boundary layer – transition layer interface and
792 the transition layer – interior interface, respectively. Correspondingly, a 0.2°C from a
793 50-60 m depth average temperature was used to locate the interior – bottom boundary
794 layer interface. (b) Light transmission profile. (c, d) O_2 saturation profiles and
795 associated absolute concentrations.

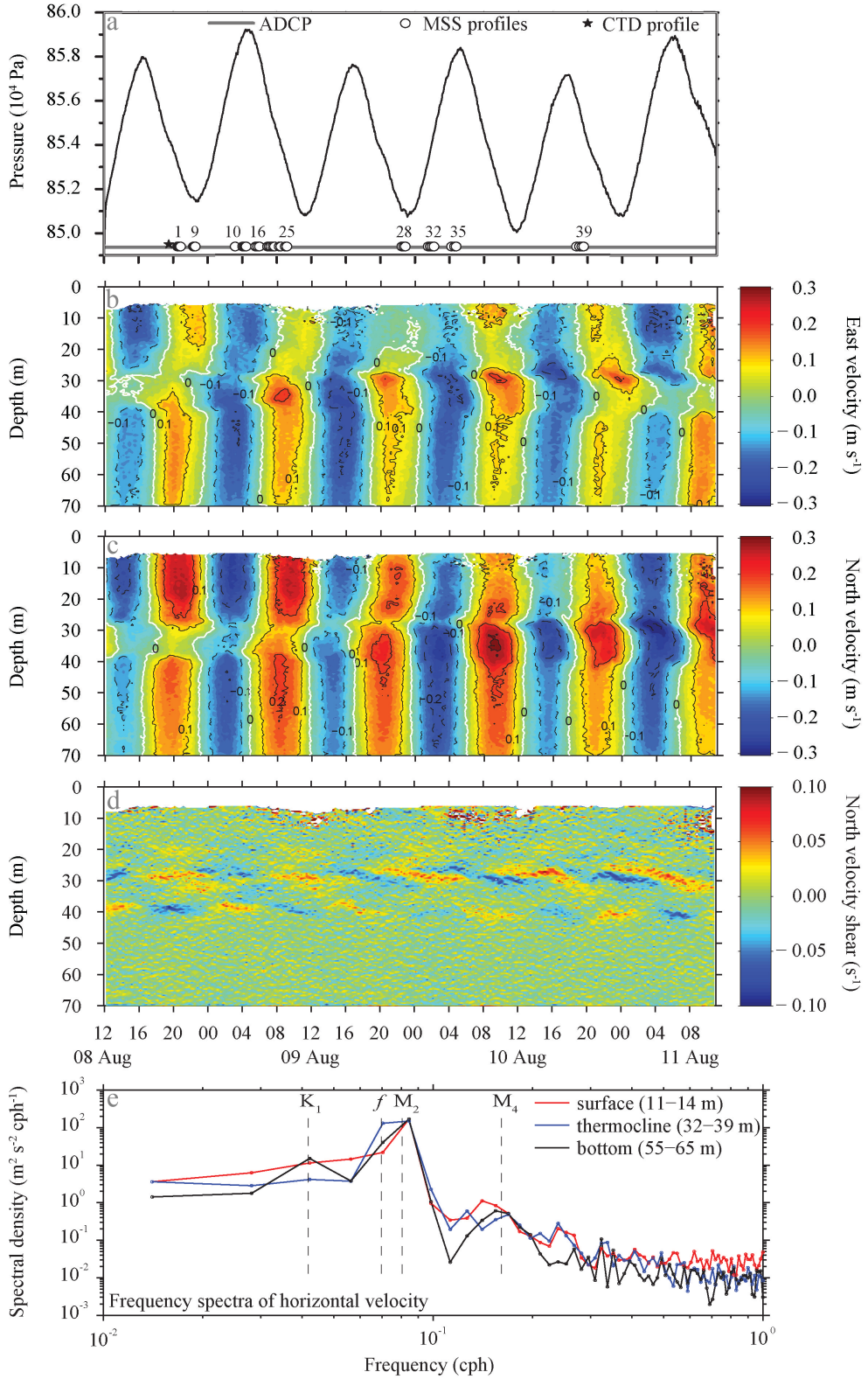

Figure 3. Current regime at the Tommeliten site from ADCP measurements (a - d) and spectral analysis (e). (a) Sea surface elevation relative to average level during the observational period (elevation = 0 m) and schedule of different instrument

deployments. Numbers on the MSS markers indicate the profile number. (b, c) Horizontal velocities, showing 20 min averaged east (b) and north (c) velocities. (d) Vertical shear of North velocity, *dv/dz*, calculated from the ADCP velocity data (see panels b, c). Note that panels a - d have the same time axis. (e) Frequency spectra of horizontal velocity calculated from the ADCP data for selected depth ranges for the SBL (surface; red line), thermocline (blue line), and BBL (bottom; black line). The inertial *f* as well as the K_1, M_2 and M_4 frequencies are marked.

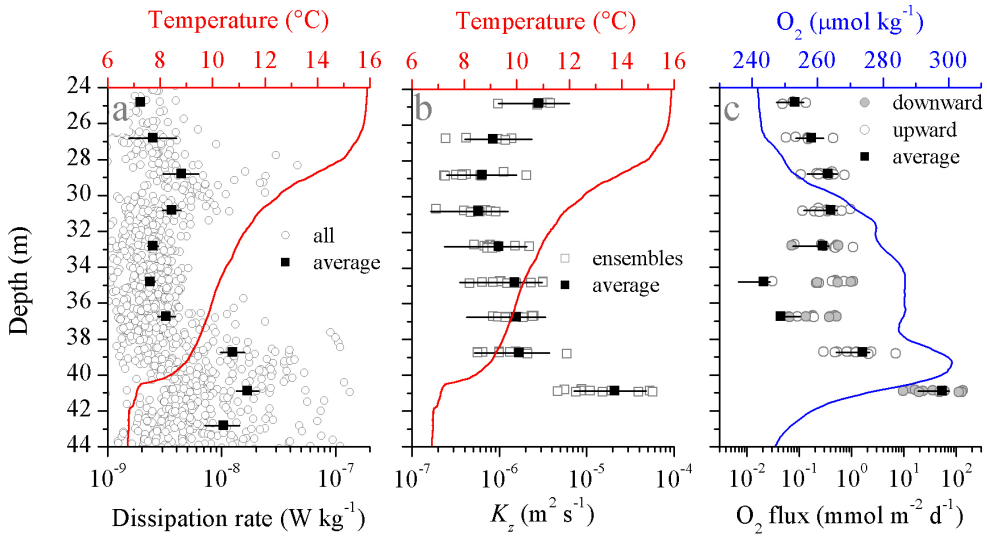

808
809

810 Figure 4. Overview of turbulent transport and O_2 fluxes within the interior (defined in
811 Fig. 2). Each panel is overlaid with temperature (a, b) and O_2 concentration (c)
812 profiles. (a) Dissipation from all profiles (open dots) together with the arithmetic
813 mean (solid squares). (b) Average vertical eddy diffusion coefficient K_z with
814 uncertainties bars as well as the K_z values for every ensemble (open squares), which
815 represent the average over 3 to 4 consecutive profiles. (c) Calculated average O_2 flux
816 over 2 m bins with the respective uncertainties intervals (solid square and black line).
817 The values for each profile cluster are shown both downward and upward fluxes (grey
818 solid and open dots, respectively). Note that in the center interior (33 – 37 m) the
819 average reflects the combination of the variability of the observed upward and
820 downwards fluxes.
821

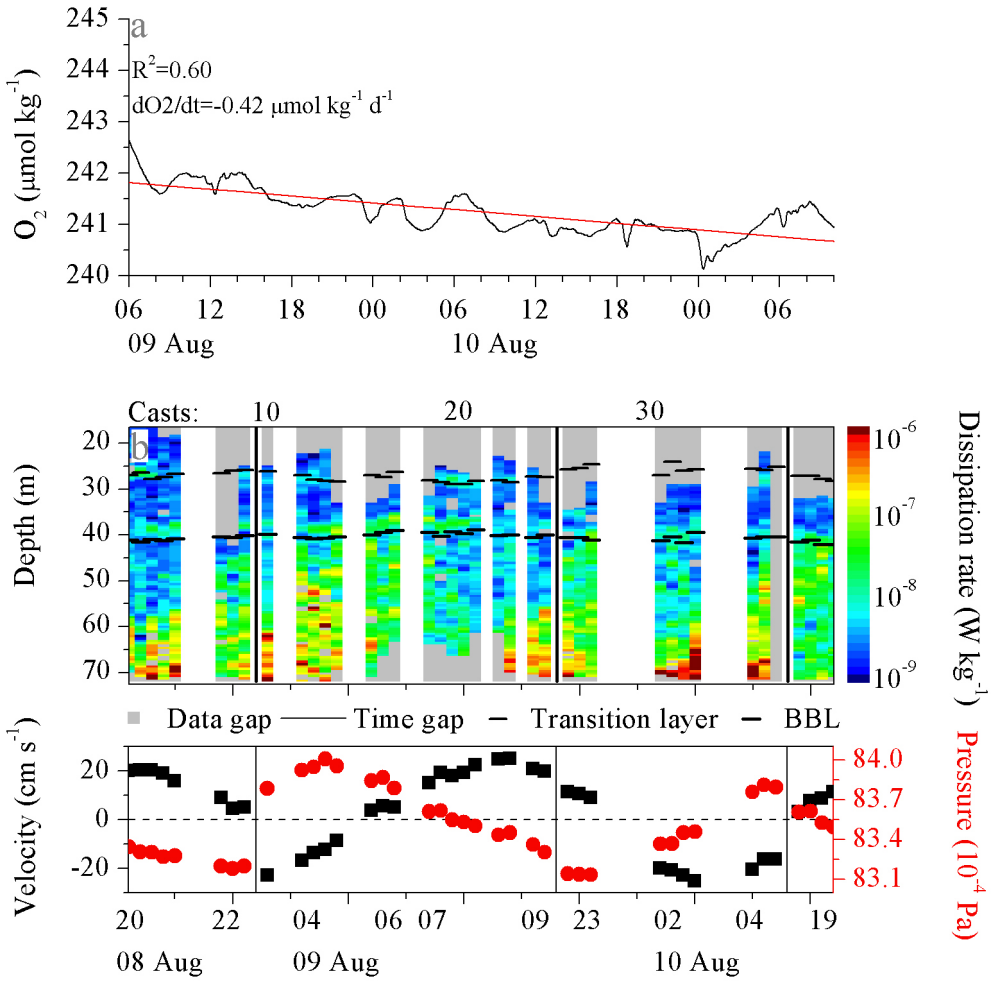

Figure 5. BBL dissolved oxygen time series and turbulence contour. (a) Near-seafloor BBL O_2 concentration changes over the observational period from the POZ-Lander. Red line indicates the estimated apparent linear O_2 loss. (b, top) Turbulence contour plot of all MSS90 casts together with the temperature layers. Thin and thick dashed lines represent the transition layer – interior interface and the interior – BBL interface, respectively. Gray spots indicate data missing due to uncompleted profiles (casts 16-23), unsuccessful profiles (cast 36), or flagged as bad based on spikes, collisions and suspected contamination due to ship activity. The vertical black lines indicate the transition (time gaps) between consecutive profile ensembles. (b, bottom) Background information on bottom current, and hydrostatic pressure during the casts. Both velocity and pressure data were collected by the deployed POZ lander. Note that as a result of the time gaps between the consecutive MSS90 casts (see Fig. 3a) the time scale is not linear.

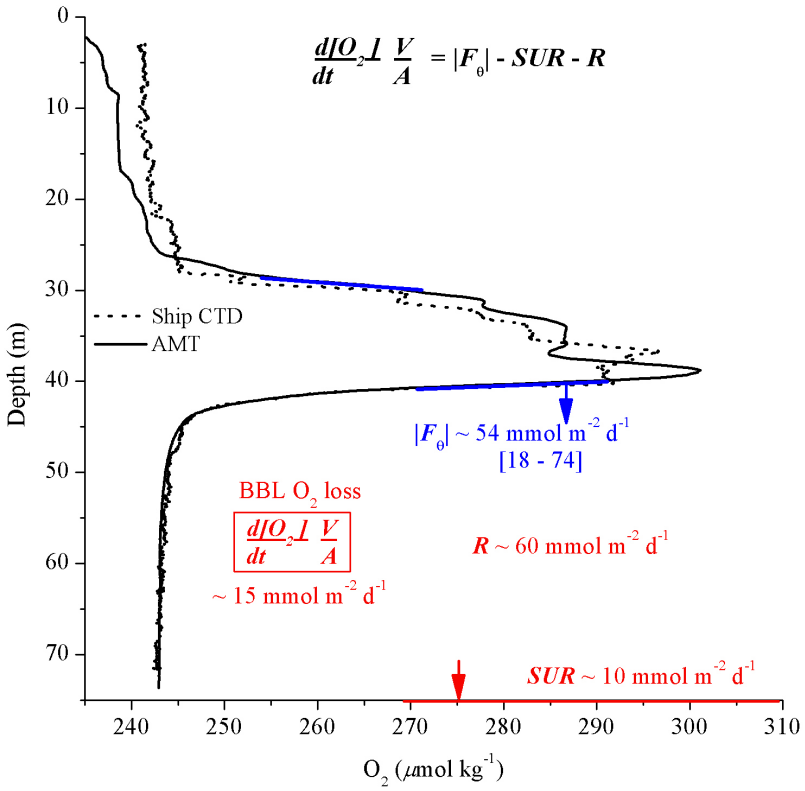

Figure 6. Main O_2 fluxes in this study. The ranges shown for the interior O_2 fluxes refer to the associated uncertainty and intermittency levels. The sediment O_2 uptake rates (SUR) are based on eddy correlation (EC) measurements (McGinnis et al., 2014), while central North Sea apparent BBL O_2 loss is based on Greenwood et al. (2010) and this study. Representative O_2 profiles are based on the AMT sensor on the MSS profiler (solid line) and ship CTD (dotted line). Note that while the O_2 profiles showed differences in absolute concentration within the thermocline, the actual O_2 gradients within the thermocline-BBL oxycline are comparable.